Konya Mühendislik Bilimleri Dergisi., c. 13, s. 4, 1232-1251, 2025
Konya Journal of Engineering Sciences v. 13, n. 4, 1232-1251, 2025
ISSN: 2667-8055 (Electronic)
DOI: 10.36306/konjes.1626828

# RETROFITTING FOR RESILIENCE: SEISMIC REHABILITATION AND LIFE CYCLE COST ANALYSIS OF A REINFORCED CONCRETE SCHOOL IN NICOSIA AFTER THE 2023 TURKEY EARTHQUAKES

**[1] Sasan BABAEI, [2,*] Fooad KARIMI GHALEH JOUGH**

*[1,2] Final International University, Engineering Faculty, Civil Engineering Department, Kyrenia, TURKISH REPUBLIC OF NORTHERN CYPRUS*

[1] sasan.babaei@final.edu.tr, [2] fooad.karimi@final.edu.tr

## *Highlights*

- Retrofitting was applied to a case study school building consisting of blocks that were initially at the collapse stage of the performance level under a maximum credible earthquake.
- Existing building Seismic rehabilitation reduced drift ratios and displacements by up to 90%.
- Retrofitted structures met immediate occupancy criteria after seismic events.
- Rehabilitation costs were less than 15% of rebuilding expenses.
- Life cycle cost analysis emphasized long-term financial benefits of retrofitting.

## *Graphical Abstract*


Process of rehabilitation and life cycle cost analysis

***Corresponding Author:** Fooad KARIMI GHALEL JOUGH, fooad.karimi@final.edu.tr

Konya Mühendislik Bilimleri Dergisi., c. 13, s. 4, 1232-1251, 2025
Konya Journal of Engineering Sciences v. 13, n. 4, 1232-1251, 2025
ISSN: 2667-8055 (Electronic)
DOI: 10.36306/konjes.1626828

# RETROFITTING FOR RESILIENCE: SEISMIC REHABILITATION AND LIFE CYCLE COST ANALYSIS OF A REINFORCED CONCRETE SCHOOL IN NICOSIA AFTER THE 2023 TURKEY EARTHQUAKES

**[1] Sasan BABAEI, [2,*] Fooad KARIMI GHALEH JOUGH**

*[1, 2] Final International University, Engineering Faculty, Civil Engineering Department, Kyrenia, TURKISH REPUBLIC OF NORTHERN CYPRUS*

[1] sasan.babaei@final.edu.tr, [2] fooad.karimi@final.edu.tr

**(Received: 25.01.2025; Accepted in Revised Form: 09.08.2025)**

**ABSTRACT:** In 2023, Turkey was hit by a devastating doublet of earthquakes, measuring 7.7 and 7.6 in magnitude, resulting in widespread destruction of residential and public infrastructure. In the aftermath, the Turkish Republic of Northern Cyprus initiated a project aimed at rehabilitating educational facilities. This paper investigates the rehabilitation efforts carried out at Atatürk Technical High School in Nicosia. To assess the building's seismic resilience, a nonlinear time-history analysis was performed using 11 mainshock-aftershock sequences to evaluate its lateral load resistance and potential plastic deformations. As part of the rehabilitation, shear walls and steel X-braced frames were added to the lateral load-resisting system, with their effectiveness being examined. Post-retrofit results demonstrate substantial improvements: maximum roof displacement and drift ratios decreased by 70 to more than 90% for different blocks and directions, and plastic hinge formation shifted predominantly to the Immediate Occupancy state. Although added stiffness led to moderate increases in floor acceleration, the retrofit strategy dramatically reduced human-related losses, with fatality costs decreasing by over 90%. The rehabilitation cost of all blocks was investigated and found to be less than 15% of rebuilding costs. While non-structural and downtime-related losses increased, overall safety- related economic outcomes were significantly enhanced.

***Keywords:*** *Case Study, Seismic Rehabilitation, School Building, Performance-based Design, Life Cycle Cost Analysis*

## 1. INTRODUCTION

Natural hazards have consistently caused significant destruction, particularly in densely populated urban areas. In the first half of 2023, earthquakes in Turkey were the primary contributors to an estimated $110 billion in global losses from natural disasters [1]. The Ministry of Treasury and Finance of Türkiye estimates the economic impact of these earthquakes at approximately $103.6 billion, representing 9% of the country's projected national income for 2023 [2]. The Kahramanmaraş earthquakes on February 6, 2023, with magnitudes of Mw 7.7 and Mw 7.6 occurring nine hours apart, resulted in over 50,000 deaths and the destruction of nearly half a million apartments across the region [3-5].

The earthquake severely affected critical infrastructure, including roads, hospitals, schools, and other essential public facilities. Although a portion of the structural failure modes in the affected regions was due to local site conditions and near-fault ground motion effects—such as large amplitude, long-period velocity pulses, intense shaking, and prolonged duration—studies in Hatay and Malatya suggest that regular lateral load-resisting systems failed primarily due to outdated building codes, substandard materials, flawed construction practices, and challenging soil and site conditions [6-13].

For example, Kazaz reported that flexural-compression and shear-compression failures in reinforced concrete frame-wall systems were primarily caused by construction issues, including inadequate seismic detailing, the absence or insufficiency of stirrups, poorly executed connections, insufficient lap splices, inadequate development lengths, and substandard concrete quality. Design shortcomings were equally significant, characterized by low wall density indices (0.2–0.4%), frame-wall interaction effects, and

***Corresponding Author:** Fooad KARIMI GHALEL JOUGH, fooad.karimi@final.edu.tr

significant axial load variations on walls. These factors collectively contributed to the deterioration of wall performance and ductility under seismic demands [14, 15].

Hospitals play a pivotal role in emergencies, requiring uninterrupted operation to treat the injured, while schools, beyond ensuring student safety, often serve as temporary shelters for displaced individuals. Given their critical functions, these buildings must be constructed and maintained to the highest safety standards. Qu et al., after investigating 12 hospitals in the affected region, found that while base-isolated hospitals remained functional, most fixed-base hospitals suffered nonstructural damage, losing immediate occupancy [16, 17].

Ozturk et al. investigated the causes of damage in 13 school buildings near the earthquake epicenter, revealing multiple factors that contributed to their destruction. Seismological analysis showed that ground accelerations in many areas exceeded design expectations, necessitating revisions to seismic codes. Poor site selection, particularly on fault lines, further exacerbated structural damage. Structural deficiencies, especially in pre-1998 buildings, were critical, with inadequate seismic detailing, weak columns, soft-story effects, and limited shear wall usage leading to significant failures. Additionally, poor construction quality, inadequate material selection, and outdated type-design projects resulted in low earthquake resistance [18].

In a similar field and numerical study by Altiok et al., poor structural design and substandard construction materials were key factors in the school collapses observed, especially in buildings constructed before 2000. Deficiencies such as brittle columns, inadequate shear walls, excessive stirrup spacing, and low-quality concrete were prevalent. However, retrofitting with reinforced concrete shear walls significantly enhanced seismic performance by minimizing displacements, drifts, and energy transfer. Simulations confirmed that retrofitted school buildings, including seven blocks across four schools, remained intact, highlighting the critical role of proper retrofitting in improving earthquake resilience, even in poorly constructed buildings [19].

While structural analysis has been extensively conducted, the economic considerations surrounding the retrofitting of buildings damaged by earthquakes, specifically life-cycle cost (LCC) analysis, play an equally significant role in the decision-making process. In recent studies, such as those by De León et al., life-cycle cost optimization has been used to assess seismic retrofitting reliability, highlighting the importance of minimizing long-term costs while ensuring the structural resilience of buildings [20]. Similarly, Kulthanaphanich et al. integrated seismic and energy retrofitting within a unified LCC framework, emphasizing the combined environmental and economic benefits of such strategies [21]. Yan et al. also demonstrated that novel hybrid bracing systems, such as self-centering viscous energy-dissipative frames, offer superior life-cycle economic benefits compared to traditional systems [22].

In response to the 2023 Turkish earthquake, the government of North Cyprus initiated a program to rehabilitate essential facilities, including schools, in several cities. This case study focuses on the rehabilitation process for Ataturk Technical High School, located in the city of Nicosia. The structural analysis of the school was conducted using 11 different earthquake ground motion records, which included both mainshock and aftershock sequences. These records, sourced from various seismic events, were scaled to match the Design Basis Earthquake (DBE) spectrum defined in the Turkish Seismic Code, ensuring that the simulation reflected realistic seismic demands for the region. The rehabilitation process involved detailed time-history analysis to assess the building's response under seismic loading, allowing for the identification of structural weaknesses and the development of appropriate retrofitting strategies. Additionally, a life-cycle cost analysis was performed to evaluate the economic impact of the retrofitting, comparing the costs associated with rehabilitation against the potential costs of damage and downtime during a major seismic event. The study evaluates the performance of the original and retrofitted school buildings, comparing key seismic response parameters such as displacement, drift ratio, and structural damage across all 11 records. The results highlight significant improvements in seismic resilience and safety through retrofitting, with the analysis demonstrating that retrofitting was a cost-effective solution, offering substantial savings compared to the potential costs of new construction or post-earthquake repairs.

## 2. DEFINITION OF THE INVESTIGATED BUILDINGS

The study focuses on a school in central Nicosia, North Cyprus. The school comprises six separate blocks, each built at various times, adhering to different building codes and material standards. These blocks include the main building, the Hairdressing School, Classroom Blocks, the Atelier, and the Kindergarten, as depicted in Figure 1.

The structure analyzed combines two different buildings. The first is a one-story kindergarten building constructed more than 30 years ago. This building is a reinforced concrete structure with columns on the first story and a mezzanine level, which contains short columns, making it susceptible to shear failures. Laboratory tests have proven that the material used is class C16 concrete, with an f'c value of 16 MPa, and the steel reinforcement has a yield strength of 220 MPa. The older structure has lower structural quality, and follows outdated code provisions, making it a suitable candidate for detailed analysis.

**Figure 1.** Ataturk Technical High School; a) Main building, b) Kindergarten c) Hairdressing School, d) Classroom Blocks, e) Atelier

The second building is a newly constructed structure added to the main buildings to accommodate more classrooms, addressing the increased demand due to the prevailing academic requirements of the school. This structure consists of two statistically independent blocks, Block A and Block B. Block A has six spans and is a two-story building. Each story contains two classrooms, and at the front, there is a corridor for students to enter. Block B has the same layout and orientation; however, it contains a staircase on the left side. The structure is built with high-quality materials, as tests have proven that the concrete compressive strength ($f'_c$) is 30 MPa, and the yield strength of the steel used is 420 MPa. The site is classified as Site Class 2, corresponding to moderately stiff soil conditions, and the seismic conditions correspond to Seismic Zone 2, indicating moderate seismicity. These conditions have been considered in the analysis, particularly with respect to the scaling of seismic records.

The rehabilitation process was carried out using the original plans and documents provided by the authorities. For the kindergarten, the plans corresponded closely with the actual structure, accurately detailing the dimensions of columns, beams, slab thicknesses, and rebar specifications. However, the official plans for classroom blocks A and B did not align with the existing structures. Consequently, the dimensions and orientations of these blocks had to be redrafted to accurately represent their current state. Figures 2 and 3 present the plan view of the kindergarten and the redrafted plan of the classroom building, respectively. The kindergarten spans 26.2 by 23.8 meters, while blocks A and B of the classroom building measure 16.2 by 10 meters and 19.3 by 10 meters, respectively.

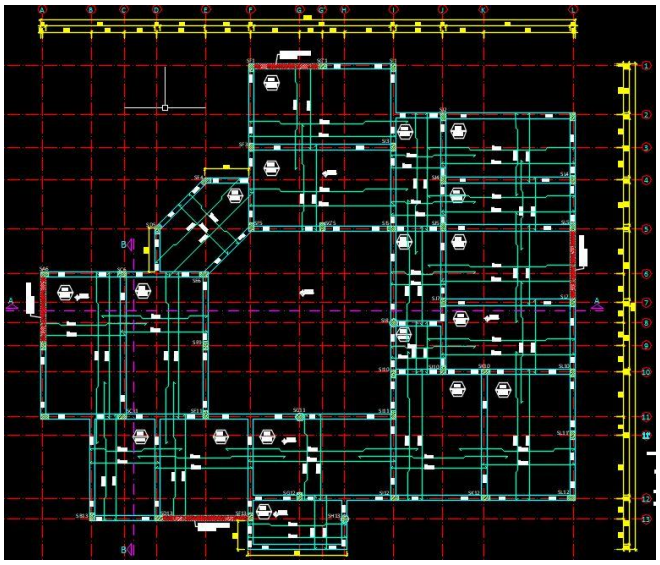

**Figure 2.** Plan view of the kindergarten building

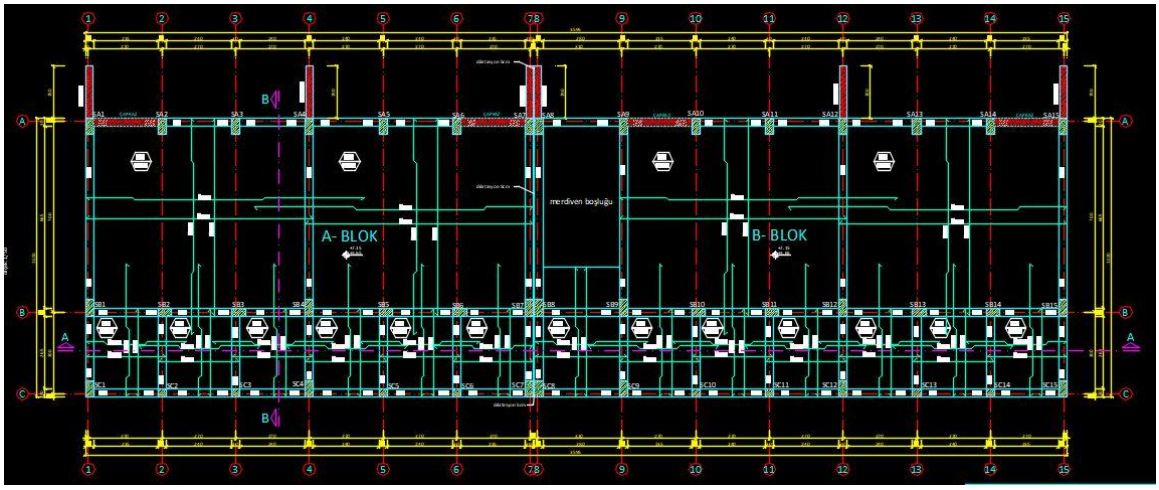


**Figure 3.** Plan view of the Classrooms Block A and B

The dimensions of the beams and columns were sourced from the government's records, as detailed in Table 1. Laboratory tests, illustrated in Figure 4, were performed to verify this data. The results indicated that the beams in the three blocks are stronger than the columns, which is suboptimal for structural design. Ideally, columns should have a greater moment of inertia to ensure that flexural deformations occur in beams rather than in columns.

**Table 1.** Dimensions and reinforcement properties of beam and columns

| Building | Element | Width (cm) | Height (cm) | Main Reinforcement | | | Stirrups |
|---|---|---|---|---|---|---|---|
| | | | | Top | Middle | Bottom | |
| Classrooms Block A and B | Column 1 | 30 | 30 | 2φ14 | 2φ14 | 2φ14 | φ8@16-19 |
| | Column 2 | 30 | 50 | 2φ16 | 2φ16 | 4φ16 | φ8@16-19 |
| | Column 3 | 30 | 60 | 3φ16 | 3φ16 | 4φ16 | φ8@16-19 |
| | Beam 1 | 30 | 60 | 4φ14 | 2φ12 | 4φ14 | φ8@17 |
| | Beam 2 | 30 | 80 | 4φ16 | 2φ12 | 4φ18 | φ8@17 |
| Kindergarten | Column 4 | 25 | 40 | 2φ14 | 2φ14 | 2φ14 | φ8@10-19 |
| | Beam 3 | 25 | 60 | 3φ12 | 2φ12 | 3φ14 | φ8@17 |
| | Beam 4 | 30 | 70 | 3φ14 | 3φ18 | 3φ18 | φ8@17 |

**Figure 4.** Laboratory test for validation; a) Extracted concrete cores for compression test; b) Scanning concrete rebars

## 3. LIFE CYCLE COST ASSESSMENT

The life-cycle cost analysis (LCCA) of a structure estimates the total expected cost CT over its design life, accounting for both initial investment and potential earthquake-induced losses. The total cost is expressed as: [23]

$$C_T = C_{In} + C^i_{dam} + C^i_{non} + C^i_{dwn} + C^i_{inj} + C^i_{fat} \quad (1)$$

where $C_{In}$, $C_{dam}$, $C_{non}$, $C_{dwn}$, $C_{inj}$, and $C_{fat}$ represent the initial investment, structural damage repair costs, non-structural losses, financial losses due to downtime and occupancy disruption, and human injury and fatality costs, respectively. The initial investment covers expenses for materials, labor, and non-structural components required for construction or renovation, while the other terms reflect the present value of costs associated with $i^{th}$ limit state. These costs include repair expenses, content losses, recovery from injuries or fatalities, and various direct and indirect economic impacts caused by earthquake-induced structural damage. Quantifying human fatality remains challenging, with approaches ranging from purely economic assessments to those acknowledging its inestimable value. Damage indices, such as drift ratio and peak floor acceleration, are commonly used to evaluate structural and non-structural damage, serving as essential parameters for loss estimation. These indices were selected based on the literature, as detailed in Table 2. [24]

**Table 2.** Drift ratio and peak floor acceleration thresholds for moment-resisting frames [25]

| Performance Level | Drift Ratio (%) | Peak Floor Acceleration (g) |
|---|---|---|
| No Damage | $\delta \leq 0.1$ | $a_f \leq 0.05$ |
| Minor | $0.1 < \delta \leq 0.2$ | $0.05 < a_f \leq 0.10$ |
| Moderate | $0.2 < \delta \leq 0.4$ | $0.10 < a_f \leq 0.20$ |
| Considerable | $0.4 < \delta \leq 1.0$ | $0.20 < a_f \leq 0.80$ |
| Severe | $1.0 < \delta \leq 1.8$ | $0.80 < a_f \leq 0.98$ |
| Extensive | $1.8 < \delta \leq 3.0$ | $0.98 < a_f \leq 1.25$ |

Non-structural loss comprises losses caused by either structural deformation ($C^{\delta}_{non}$) or floor acceleration ($C^{acc}_{non}$), as presented in Equation 2.

$$C^{i}_{non} = C^{i,\delta}_{non} + C^{i,acc}_{non} \quad (2)$$

Damage indices, socio-economic parameters, occupancy levels, and building-specific metrics are used to calculate these values. Loss functions are scaled based on the total floor area, projected damage severity, and occupancy density. Cost estimation parameters were adopted using property valuations from the Turkish Republic of Northern Cyprus (TRNC), combined with contemporary human life and injury cost guidelines from standards such as ATC-13, FEMA-227, and OECD. [26-28]

**Table 3.** Cost estimation methods for different loss scenarios in financial values.

| Cost Type | Calculation Method | Base Cost |
|---|---|---|
| Structural Damage ($C_{dam}$) | Rebuilding cost × total floor area × average damage ratio | 1200 USD/m² |
| Non-Structural Loss ($C_{non}$) | Value per unit area × total floor area × average damage index | 400 USD/m² |
| Operational Downtime Cost ($C_{dwn}$) | Rental value × rentable area × estimated downtime | 1000 USD/m² |
| Minor Injuries ($C_{inj,m}$) | Cost × area × occupancy × projected minor injury rate | 3000 USD/person |
| Severe Injuries ($C_{inj,s}$) | Cost per severe injury × total floor area × occupancy rate × projected severe injury rate | 35,000 USD/person |
| Fatalities ($C_{fat}$) | Cost × area × occupancy × projected severe injury rate | 5.0 million USD/person |

* Injury and fatality cost estimates are aligned with OECD VSL and WHO global injury burden data. An occupancy level of 30 students per 100 m² was assumed, reflecting typical educational occupancy in TRNC.

**Table 4.** Parameters for cost assessment based on structural performance levels

| Performance Level | FEMA-227 | | | | ATC-13 |
|---|---|---|---|---|---|
| | Average Damage Index (%) | Projected Minor Injury Rate | Projected Severe Injury Rate | Estimated Fatality Rate | Operational Downtime (%) |
| No Damage | 0 | 0 | 0 | 0 | 0 |
| Minor | 0.5 | 3.0E-05 | 4.0E-06 | 1.0E-06 | 0.9 |
| Moderate | 5 | 3.0E-04 | 4.0E-05 | 1.0E-05 | 3.33 |
| Considerable | 20 | 3.0E-03 | 4.0E-04 | 1.0E-04 | 12.4 |
| Severe | 45 | 3.0E-02 | 4.0E-03 | 1.0E-03 | 34.8 |
| Extensive | 80 | 3.0E-01 | 4.0E-02 | 1.0E-02 | 65.4 |
| Complete Failure | 100 | 4.0E-01 | 4.0E-01 | 2.0E-01 | 100 |

## 4. TIME HISTORY ANALYSIS

As outlined by the Ministry of Education, the rehabilitation approach began with a pushover analysis. While this technique is widely used and reliable, it has inherent limitations in fully representing the nonlinear behavior of structures, particularly in relation to the frequency characteristics of seismic records. Furthermore, pushover analysis does not adequately account for the effects of ground motion duration or

the sequential development of hinge formations, which can be better captured through time history analysis.

A total of 11 earthquake ground motion records, including mainshock–aftershock sequences and doublet events, were selected for the nonlinear time history analysis of the case study structure. These records were compiled from a variety of publicly available strong-motion databases, including the AFAD TDAS Strong Motion Database, Kandilli Earthquake Research Institute Database, the PEER NGA-West2 Database, the COSMOS Virtual Data Center, the ITACA Strong Motion Database (Italy), the IRIS Ground Motion Archive, and the New Zealand GeoNet Strong Motion Database. All ground motions were scaled to match the Design Basis Earthquake (DBE) spectrum defined in the Turkish Seismic Code (TBDY- 2018) [29]. The structure is located in Seismic Zone 2, and the local soil condition is classified as Type 2 (ZC), corresponding to medium-stiff ground. The scaling process ensures consistency with code-based seismic demand at the site, and minimizes the influence of original ground motion variability on the structural response.

**Table 5.** Summary of Parameters for Selected Earthquake Ground Motion Sequences

| Event | Sequence | M | Year | Name/ID | Site Class | PGA (g) |
|---|---|---|---|---|---|---|
| Kahramanmaraş | MS | 7.7 | 2023 | Pazarck/-1 | C | 0.122 |
| | AS | 7.6 | | Elbistan/ 15537 | C | 0.523 |
| İzmit | MS | 7.4 | 1999 | Kocaeli | D | 0.230 |
| | AS | 7.2 | | Düzce | D | 0.018 |
| Superstition Hills | MS | 6.22 | 1987 | Superstition Hills-01 | - | 0.25 |
| | AS | 6.54 | | Superstition Hills-02 | - | 0.375 |
| Elazığ | MS | 6.8 | 2020 | 202001241755/ Elazig | B | 0.293 |
| | AS | 5.4 | | 8502 | C | 0.0143 |
| Ridgecrest | MS | 7 | 2019 | Ridgecrest - 395/Brown Road Bridge | C | 0.243 |
| | AS | 6.4 | | Searles Valley, CA | C | 0.260 |
| Amatrice | MS | 6.0 | 2016 | Amatrice Earthquake | B | 0.868 |
| | AS | 5.9 | | Campi Earthquake | C | 0.651 |
| Umbria & Marche | MS | 5.7 | 1997 | IT-1997-0004 | E | 0.256 |
| | AS | 6.0 | | IT-1997-0006 | E | 0.430 |
| Van | MS | 6.7 | 2011 | 201110231041 | - | 0.172 |
| | AS | 5.6 | | 201111091923 | - | 0.243 |
| Emilia | MS | 6.1 | 2012 | 20120520 | C | 0.262 |
| | AS | 6.0 | | 3911 | C | 0.420 |
| Dusky Sound | MS | 7.8 | 2009 | 3124785 | - | 0.147 |
| | AS | 6.1 | | 3308618 | | 0.008 |
| Kaikōura | MS | 6.7 | 2016 | 2016p859524 | - | 0.245 |
| | AS | 5.7 | | 2016p860224 | - | 0.051 |

To address plastic deformations and hinge formation in primary structural elements, the guidelines outlined in Table 10.8 and Table 10.9 of ASCE 41-17 were applied for columns, while Table 10.7 was utilized for beams. (ASCE/SEI 41-17, 2017). These parameters were integrated into the structural model through the hinge definitions available in SAP2000 [30].

## 5. REHABILITATION TECHNIQUE

The design incorporates rehabilitation techniques such as a 25-centimeter-thick shear wall or an X-brace frame made of rectangular tube sections measuring 200 cm with a 10 cm thickness. ST275-grade steel was chosen for these sections based on its availability in the Cyprus market. The connection between the old and new concrete is achieved through the use of Hilti anchors, which secure reinforcement bars at regular intervals, ensuring effective bonding. The steel braces are connected to the concrete frame via steel plates, which are bolted securely to transfer axial forces and enhance structural stability.

The rehabilitated model of the building is illustrated in Figure 5 for the kindergarten structure. As

shown, four shear walls were added to enhance lateral resistance, with two walls in the X-direction and two in the Y-direction to provide adequate lateral resistance in both directions. Figure 6 further illustrate the shear wall and brace frames added to the lateral load-resisting system for Blocks A and B. Three shear walls, each 2 meters long, were added in the Y-direction for both blocks, while two X-brace frames were added in the X-direction to ensure sufficient lateral resistance for each block. Additionally, the two structures now share a joint foundation.

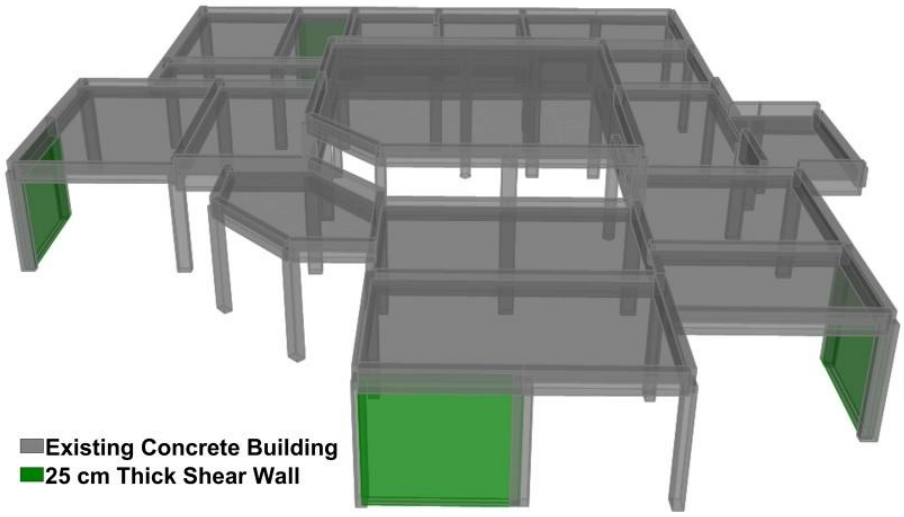


**Figure 5.** Rehabilitated building kindergarten

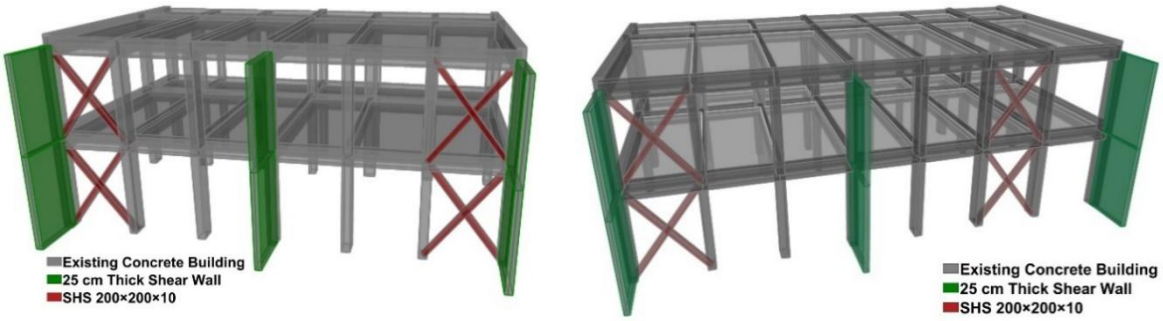


**Figure 6.** Rehabilitated building classrooms a) Block A, b) Block B

The implementation of the shear walls and hollow steel tube sections in these structures is depicted in Figures 7 and 8.

**Figure 7.** Shear wall added to classroom, a) Block B, b) Block A

**Figure 8.** Tube 200x200x12.5 X-braced frames added to classroom, a) Block A, b) Block B

## 6. COMPARISON OF SEISMIC RESPONSE IN EXISTING AND RETROFITTED STRUCTURES

To assess the seismic performance improvement due to retrofitting, nonlinear time-history analyses were performed on three representative structures—Block A, Block B, and the kindergarten building—subjected to 11 selected earthquake ground motion records in both the X and Y directions.

Figure 9 displays the roof displacement time histories in the X and Y directions for both the existing and rehabilitated configurations of the kindergarten under the 2023 Kahramanmaraş (Türkiye) earthquake record. In the X direction, the peak roof displacement of the existing structure reached 3.488 cm, whereas the rehabilitated version showed a significantly reduced displacement of 2.27 mm—corresponding to a reduction of approximately 93.5%. Similarly, in the Y direction, displacement decreased from 2.37 cm to 2.91 mm, representing a reduction of about 87.7%. This substantial decrease in lateral drift is primarily attributed to the introduction of large shear walls in both directions, which significantly increased the lateral stiffness and deformation control capacity of the structure.

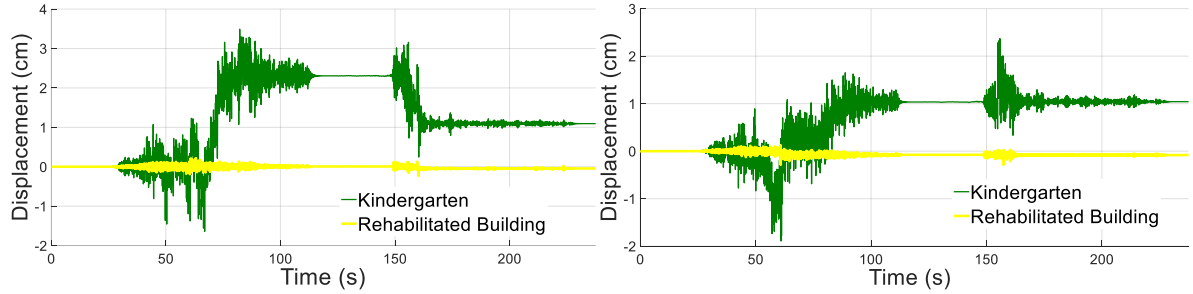


**Figure 9.** Time-history roof displacement for the kindergarten structure in a) X, b)Y directions

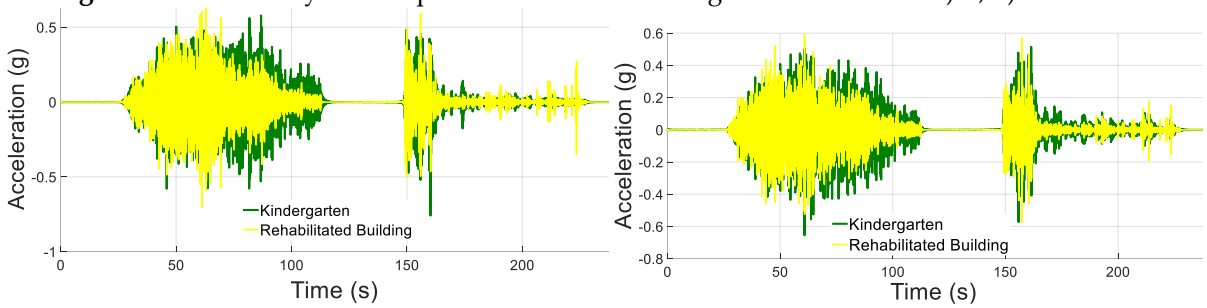


**Figure 10.** Time-history roof acceleration for the kindergarten structure in a) X, b)Y directions

In terms of acceleration response, no significant change was observed between the existing and retrofitted cases for this specific record. The peak roof accelerations remained relatively consistent in both directions, as shown in Figure 10, suggesting that the rehabilitation primarily affected displacement behavior without noticeably increasing acceleration demands.

Table 6 summarizes the dynamic characteristics and seismic response parameters of three structural units—Kindergarten, Block A, and Block B—each evaluated in both their existing and rehabilitated states. The comparison spans key performance metrics such as natural period, maximum roof displacement, residual drift, drift ratio, and floor acceleration in both principal directions (X and Y). The overall trend reveals that rehabilitation strategies, including the addition of shear walls and braced frames, significantly improved the seismic behavior of all buildings. In particular, structural stiffness increased, leading to shorter natural periods and lower displacement-related demands. This effect is most pronounced in the Kindergarten building, where the maximum roof displacement in the X direction decreased from 10.7 cm to 0.45 cm, and the residual drift dropped from 11.10 mm to 0.27 mm highlighting the profound impact of retrofitting.

Upon closer inspection, the table reveals a number of discrepancies and directional sensitivities that carry structural significance. For instance, in Block A and Block B, the Y-direction tends to show greater relative improvement, particularly in drift and displacement parameters. This can be attributed to the retrofit design, which incorporated three shear walls in the Y direction of both blocks—effectively enhancing lateral stiffness in that axis. Conversely, the X direction, where only two braced frames were introduced and the span of columns is wider, shows comparatively less dramatic improvement. Moreover, the existing column orientation further contributes to this asymmetry: the column layout in Blocks A and B favors the Y direction in stiffness, which in the existing condition already offered better seismic resistance. As such, the retrofitting benefits in the X direction, though significant, are not as extensive due to inherent geometric limitations and weaker pre-existing stiffness in that direction.

**Table 6.** Dynamic characteristics and engineering response parameters of existing and rehabilitated building's blocks

| Building | Direction | Kindergarten | | Block A | | Block B | |
|---|---|---|---|---|---|---|---|
| | | Existing | Rehabilitated | Existing | Rehabilitated | Existing | Rehabilitated |
| Period (s) | X | 0.262 | 0.058 | 0.267 | 0.166 | 0.264 | 0.18 |
| | Y | 0.239 | 0.08 | 0.203 | 0.12 | 0.201 | 0.13 |
| Max Roof Displacement (cm) | X | 2.94 | 0.265 | 1.996 | 0.871 | 2.18 | 1.024 |
| | Y | 2.51 | 0.265 | 1.257 | 0.364 | 1.128 | 0.486 |
| Residual Drift (mm) | X | 10.7 | 0.45 | 4.407 | 0.126 | 5.627 | 0.238 |
| | Y | 11.1 | 0.265 | 1.573 | 0.001 | 1.668 | 0.03 |
| Drift Ratio (δ%) | X | 0.9 | 0.079 | 0.453 | 0.121 | 0.524 | 0.171 |
| | Y | 0.766 | 0.072 | 0.238 | 0.031 | 0.205 | 0.056 |
| Floor Acceleration (g) | X | 0.556 | 1.005 | 0.8 | 1.018 | 0.862 | 1.165 |
| | Y | 0.535 | 0.979 | 0.77 | 0.658 | 0.939 | 1.07 |

The Kindergarten building demonstrates the highest magnitude of change, which aligns with its original vulnerability and the use of outdated structural code practices. Its rehabilitation under modern seismic codes, through the incorporation of shear walls only, yielded substantial improvements in stiffness, deformation capacity, and drift control. For instance, the drift ratio in the Y direction dropped from 0.77% to 0.07%, indicating a nearly 91% reduction. Interestingly, although displacement metrics uniformly decreased post-retrofit, floor accelerations in some cases increased—such as in Block B (X direction), where the value rose from 0.86 g to 1.17 g. This is consistent with the expected dynamic relationship a=w2x, where increased stiffness leads to higher natural frequency and thus higher acceleration, even as displacements reduce. These patterns not only validate the retrofit approach but also highlight the complex trade-offs involved in seismic strengthening, particularly between controlling deformation and managing acceleration-sensitive components.

To capture the variability and directional sensitivity of the structural response under multiple ground motion scenarios, a series of radar charts are provided for the Kindergarten, Block A, and Block B structures as shown at Figures 11 to 14. These charts present the maximum roof displacement, residual drift, drift ratio, and floor acceleration for both existing and rehabilitated configurations in the X and Y directions, evaluated across all 11 selected earthquake records. The radar charts serve as a visual representation of the sensitivity analysis, illustrating how each structure responds to different seismic inputs and how retrofitting measures affect performance across directions and demand parameters.

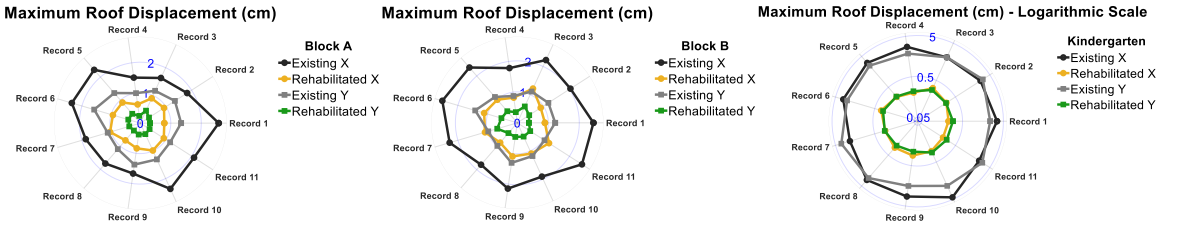


**Figure 11.** Maximum roof displacement for existing and rehabilitated buildings under 11 seismic records in X and Y directions, a) Blocks A, b) Block B, and c) Kindergarten.

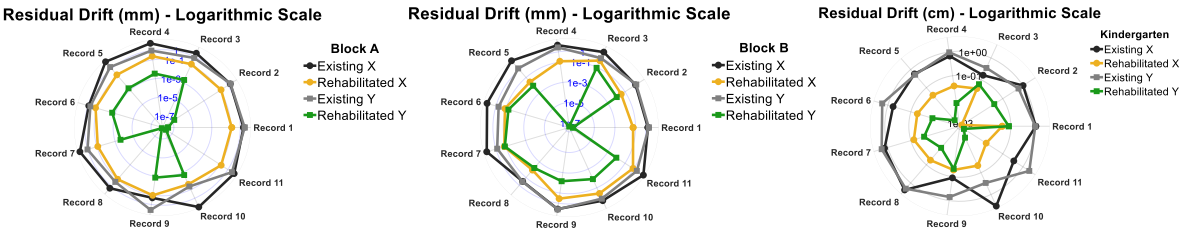


**Figure 12.** Residual drift for existing and rehabilitated buildings under 11 seismic records in X and Y directions, a) Blocks A, b) Block B, and c) Kindergarten.

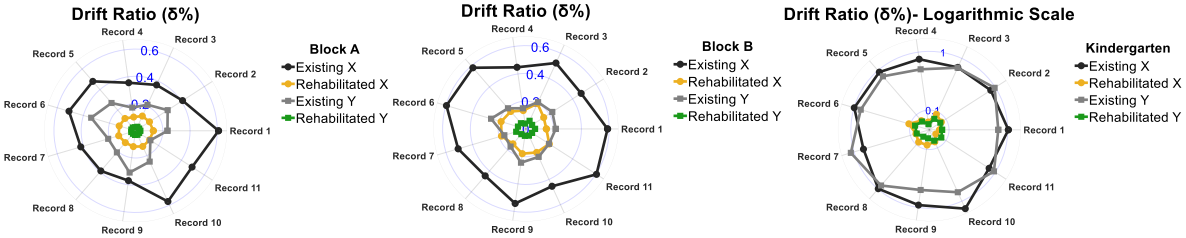


**Figure 13.** Drift Ratio (%) for existing and rehabilitated buildings under 11 seismic records in X and Y directions, a) Blocks A, b) Block B, and c) Kindergarten.

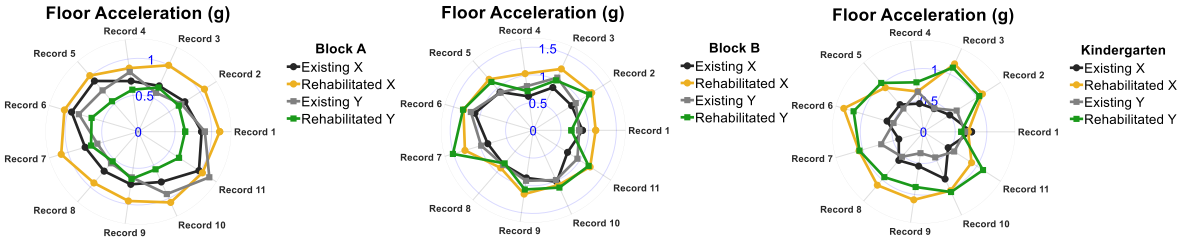


**Figure 14.** Maximum roof acceleration (g) for existing and rehabilitated buildings under 11 seismic records in X and Y directions, a) Blocks A, b) Block B, and c) Kindergarten.

To provide a comparative perspective, hinge formation was evaluated across three buildings, subjected to 11 seismic records in both the X and Y directions. Figure 15 illustrates the hinge formation in the kindergarten building following the mainshock (MS) of the Kahramanmaraş earthquake and the subsequent aftershock sequence (MS+AS). In the X direction, after the mainshock, the columns had 32 hinges in the 'life safety' state and 13 in the 'collapse' state. After the aftershock, the 'life safety' hinges remained at 32, while the number of 'collapse' hinges increased to 14. In the Y direction, after the mainshock, the columns had 20 hinges in 'life safety' and 21 in 'collapse,' which remained constant at 21. This indicates that subjecting the structure to the aftershock sequence did not push the structure much further for this specific event.

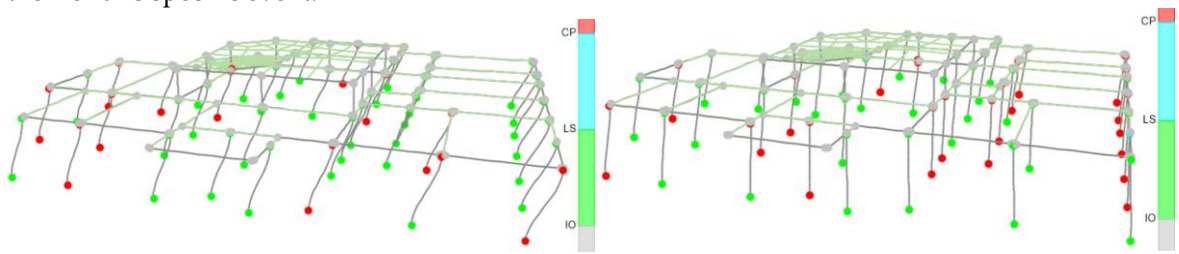


**Figure 15.** Hinge formations in the frames of the kindergarten at the end of the seismic sequences; a) X direction, b) Y direction

It is noteworthy that no hinge formation was observed in the beams of any of the buildings, likely due to their larger cross-sectional dimensions compared to the columns. The greater resistance to deformation in the beams left the columns more vulnerable to hinge formation, providing a new perspective on the behavior of structural elements during seismic events

To comprehensively assess the buildings' seismic performance, the hinge formation was depicted through scatter charts, illustrating the number of hinges at each limit state for each direction. These charts represent the differences in hinge formation across the seismic records and under various levels of acceleration.

The scatter distribution for Block A, presented in Figure 16, shows notable variability in hinge formation across different ground motion records. In the existing structure, the X-direction under Life Safety (LS) conditions displays a broad spread, with several records producing hinge counts from around 7 to over 20. Some values are tightly clustered, indicating repeated high-damage responses across different records. In the Y-direction, the existing structure exhibits concentrated Collapse-state hinge formation,

with values frequently reaching 8 to 10 hinges. After rehabilitation, the patterns shift significantly. Both X and Y directions show hinge counts condensed near Immediate Occupancy (IO), with almost no hinges in LS or Collapse states. The Y-direction, enhanced with three shear walls, shows a particularly uniform distribution post-retrofit, suggesting both a reduction in damage and high consistency across records.

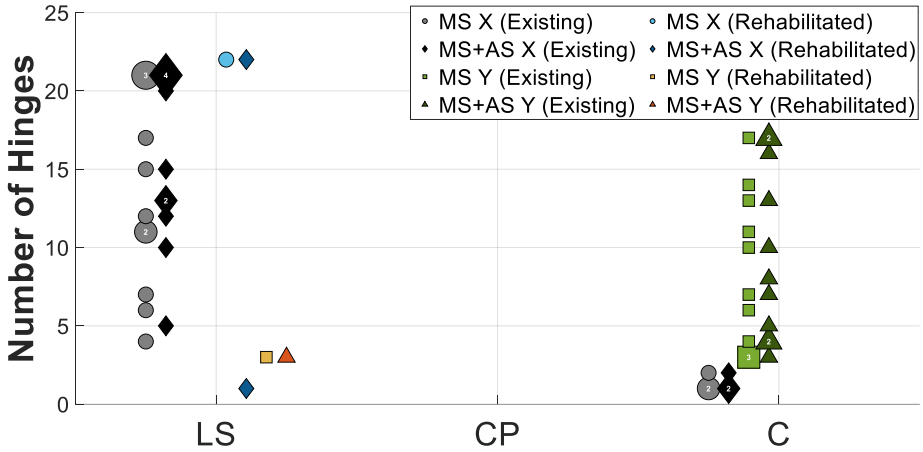


**Figure 16.** Number of plastic hinges formed at each performance limit state (LS, CP, C) for existing and rehabilitated Block A, subjected to 11 seismic sequences in both X and Y directions

Block B demonstrates similar record-to-record variability in the existing configuration as shown in Figure 16. In the X-direction, the LS hinge count ranges widely, with many records forming between 10 and 25 hinges. The Y-direction shows consistent Collapse-state hinge formation, with multiple records producing values near or above 5 hinges, and minimal variation in LS or CP states. Following rehabilitation, the X-direction (retrofitted using braced frames) still retains a few outliers—one or two records continue to form hinges in the Collapse state—although most values shift to IO. In contrast, the Y-direction, retrofitted with three shear walls, shows complete elimination of Collapse hinges and clustering of all records within the IO state. This visual contrast reinforces the higher effectiveness and consistency of shear walls under sequential loading compared to braced frames.

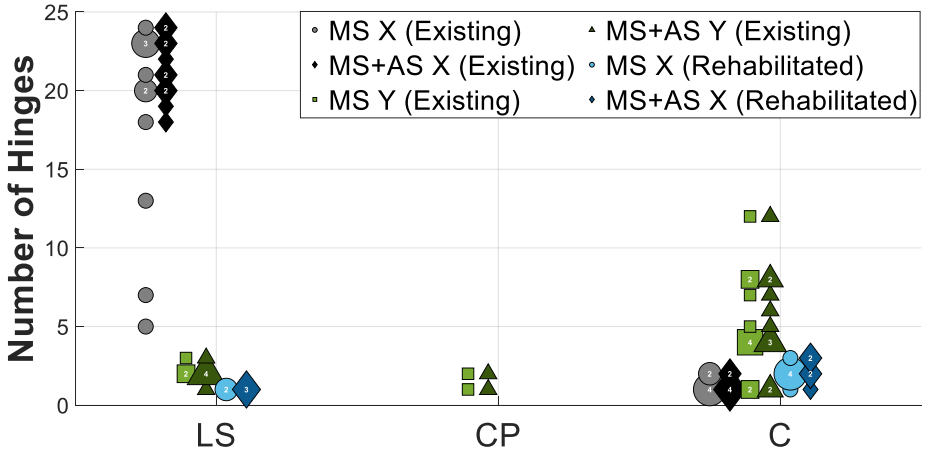


**Figure 17.** Number of plastic hinges formed at each performance limit state (LS, CP, C) for existing and rehabilitated Block B, subjected to 11 seismic sequences in both X and Y directions.

The kindergarten building shows the highest variability among the three structures, particularly in the existing condition (see Figure 18). The Y-direction exhibits substantial hinge formation in the Collapse state, with several records reaching over 20 hinges. The X-direction also shows dense clustering in the LS range, with Collapse hinges frequently appearing. After retrofitting—using two shear walls in each

direction—the hinge distribution shifts considerably toward IO. Most records now cluster at or near IO, although one or two still produce hinges in the Collapse state, especially under MS+AS sequences in the Y-direction. Compared to Blocks A and B, the kindergarten's scatter plots suggest that the reduced number of shear walls (only two per direction) may limit the uniformity of performance improvement, leading to slightly higher residual hinge formation under some ground motions.

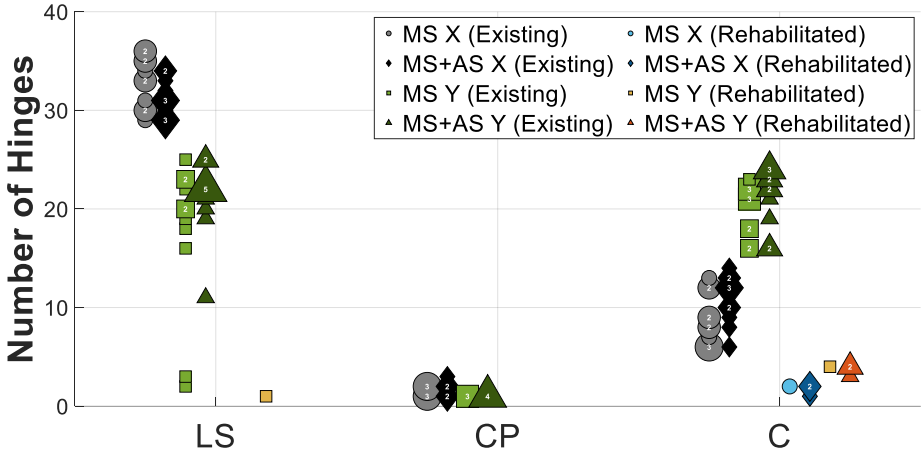


**Figure 18.** Number of plastic hinges formed at each performance limit state (LS, CP, C) for existing and rehabilitated kindergarten, subjected to 11 seismic sequences in both X and Y directions.

On average as shown on table 7, in Block A, the existing structure subjected to MS and MS+AS sequences exhibits hinge concentration primarily in the Life Safety (LS) and Collapse (C) states. In the X-direction, hinges are distributed largely within the LS range (13.27 under MS and increasing to 15.63 under MS+AS), while Collapse hinges are nearly absent. However, in the Y-direction, where no LS hinges are observed, the structure undergoes significant Collapse-state formation (8.27 under MS, increasing to 9.45 under MS+AS). After retrofitting with braced frames in the X-direction and three shear walls in the Y-direction, hinge formation shifts decisively toward Immediate Occupancy (IO) across both axes. In particular, the Y-direction exhibits complete suppression of Collapse hinges post-retrofit. While the X-direction shows comparable improvement, the residual presence of LS hinges suggests a more localized response pattern, possibly influenced by the flexibility and energy dissipation characteristics of the braced system. Notably, the decision to implement braced frames in the X-direction was influenced by foundational constraints that precluded the use of large-footprint shear walls.

**Table 7.** Average number of plastic hinges at each performance level (IO, LS, CP, C) at the end of MS and MS+AS sequences in X and Y directions for existing Block A, Block B, and the kindergarten

| Building | Direction | Record | Immediate occupancy | Life safety | Collapse prevention | Collapse |
|---|---|---|---|---|---|---|
| **Block A** | **X** | MS | 28.3 | 13.3 | 0 | 0.4 |
| | | MS+AS | 26 | 15.6 | 0 | 0.4 |
| | **Y** | MS | 33.7 | 0 | 0 | 8.3 |
| | | MS+AS | 32.5 | 0 | 0 | 9.5 |
| **Block B** | **X** | MS | 29.4 | 17.9 | 0 | 0.7 |
| | | MS+AS | 26 | 21.4 | 0 | 0.7 |
| | **Y** | MS | 42 | 0.6 | 0.3 | 5.3 |
| | | MS+AS | 42 | 1.1 | 0.3 | 5.5 |
| **kindergarten** | **X** | MS | 10.6 | 32.9 | 0.8 | 8.7 |
| | | MS+AS | 10.2 | 31.2 | 0.8 | 10.8 |
| | **Y** | MS | 15.4 | 17.4 | 0.3 | 20 |
| | | MS+AS | 10.4 | 21 | 0.4 | 21.3 |

Block B shows a similar hinge behavior in the existing structure. The X-direction is dominated by LS hinges (17.9 in MS and 21.4 in MS+AS), with minor but consistent presence of Collapse-state hinges (~0.7).

In contrast, the Y-direction experiences over 5 hinges in the Collapse state under both sequences, with negligible LS or CP contribution. Retrofitting through braced frames in the X-direction and shear walls in the Y-direction shifts the hinge distribution strongly toward IO, particularly in the Y-axis where Collapse hinges are fully eliminated and the structure achieves near-complete elastic behavior (48 IO hinges). The X-direction exhibits similar improvement, although a small number of Collapse hinges persist. These results align with the directional retrofitting strategies: while shear walls significantly increase global stiffness and control displacement, the braced frames in the X-direction—selected with practical site constraints in mind—provide effective drift limitation but may still permit localized hinge development under severe loading.

In the kindergarten building, where only shear walls were used (two per direction), the existing configuration exhibits widespread hinge formation, especially in the Y-direction under MS+AS where over 21 Collapse hinges are observed. The X-direction, while slightly better, still shows substantial LS and Collapse hinge presence. Following retrofitting, the structure's performance improves across all directions and sequences, with hinge formation overwhelmingly concentrated in the IO range and a sharp reduction in higher damage states. However, compared to Blocks A and B, the kindergarten maintains a slightly higher residual hinge count at Collapse (1 hinge in MS+AS Y-direction), which could be attributed to the limited number of shear walls and possible irregularities in geometry or mass distribution. Nevertheless, the performance enhancement across the board confirms the effectiveness of targeted retrofitting, especially in transforming Collapse-state hinges into recoverable performance zones.

## 7. REHABILITATION COST

To evaluate the applicability of the project from a comparative perspective, the rehabilitation cost of three blocks has been compared to the cost of erecting a new construction with the same performance level. The rehabilitation cost of the blocks has been calculated by considering all aspects of the project, including site excavation, site preparedness, and the rehabilitation process itself. Site excavation corresponds to creating a new foundation or enlarging existing ones. This project involves both pad footings and strip foundations. Site preparedness entails demolishing the brick walls where shear walls and braced frames are to be added to enhance the lateral load-resisting system of the building. The unit costs for these parameters, obtained from the construction sector in the Turkish Republic of Northern Cyprus at the time of the project, are provided in Table 8. This table also includes the quantities of each parameter for the three buildings.

**Table 8.** Construction Activities and Material Quantities with Unit Costs

| Activity | Unit | Kindergarten (Qty) | Classroom Block A (Qty) | Classroom Block B (Qty) | Unit Cost (USD) |
|---|---|---|---|---|---|
| Excavation | $m^3$ | 25 | 15 | 20 | 80 |
| Brick Wall Demolishing | $m^2$ | 28 | 32 | 32 | 70 |
| Blinding Concrete | $m^3$ | 3 | 3 | 3 | 110 |
| Concrete (C30) | $m^3$ | 26 | 22 | 26.5 | 160 |
| Concrete Reinforcement | ton | 3.26 | 2.98 | 3.01 | 1600 |
| Form Work | $m^2$ | 100 | 110 | 110 | 25 |
| Epoxy | $m^2$ | 16 | 12 | 12 | 600 |
| Structural Steel | ton | N/A | 4.04 | 4.04 | 4200 |
| Painting | $m^2$ | 110 | 120 | 120 | 55 |
| Cladding works | $m^2$ | N/A | 75 | 75 | 105 |
| Coating works | 1 set | N/A | 1 | 1 | 3400 |

The cost comparison across all sectors for three buildings is presented in Figure 19. Structural steel accounts for the highest percentage of construction costs. In contrast, the use of concrete shear walls in the Kindergarten results in the lowest material expenses, making it the most cost-effective option. The total

rehabilitation costs for the Kindergarten, Classroom Block A, and Block B are $31,816, $56,851, and $58,019, respectively. In comparison, constructing new projects for these one- and two-story structures, with gross floor areas of 463.4 m², 167.5 m², and 199.2 m², would cost approximately $556,000, $402,000, and $478,000, respectively. Therefore, rehabilitating each block is highly cost-effective, accounting for only 5.7%, 14.1%, and 12.1% of the cost of building new structures.

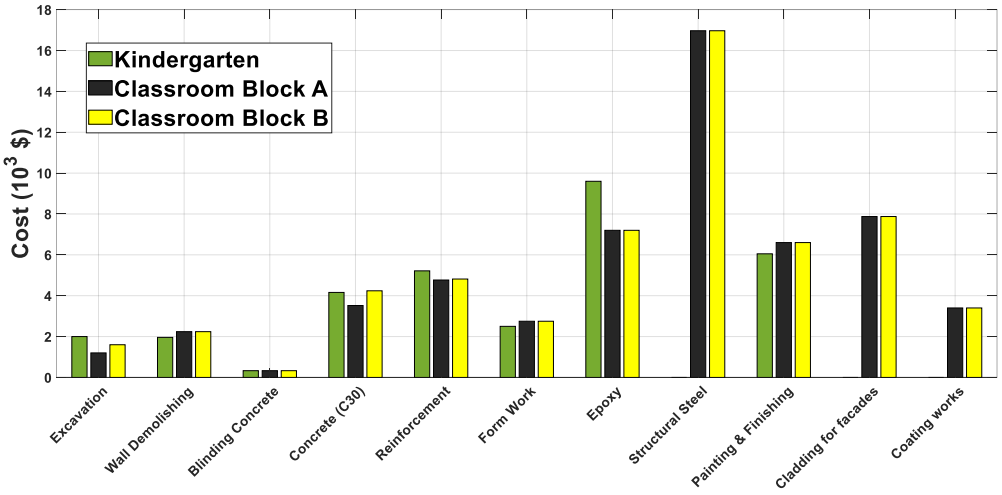


**Figure 19.** Construction cost comparison across building types and categories

## 8. LIFE CYCLE COST

The engineering demand parameters for the existing and rehabilitated buildings, including interstory drift and floor acceleration, were calculated from the time history analysis and earlier presented in Table 6. These parameters were used as inputs for the life-cycle cost analysis. In this study, it was assumed that a significant earthquake event is imminent, and the remaining lifespan of the structures is 30 years. Costs across various sectors, such as structural damage, non-structural loss, financial loss, and human impacts, were calculated for both the existing and rehabilitated buildings, as shown in Table 9. For the rehabilitated buildings, the initial cost was assigned solely to the rehabilitation process.

**Table 9.** Detailed comparison of life cycle costs for existing and rehabilitated buildings

| **Cost** | **Kindergarten** | | **Block A** | | **Block B** | |
|---|---|---|---|---|---|---|
| | Existing | Rehabilitated | Existing | Rehabilitated | Existing | Rehabilitated |
| Initial Cost | N/A | 31816 | N/A | 56851 | N\A | 58019 |
| Damage | 111216 | 0 | 80400 | 2010 | 95616 | 2390 |
| Non Structral Loss | 37072 | 148288 | 26800 | 107200 | 71712 | 127488 |
| Downtime Cost | 57462 | 303064 | 41540 | 219090 | 138643 | 260554 |
| Minor Injury | 12512 | 0 | 904 | 9 | 1076 | 11 |
| Severe Injury | 1946 | 0 | 1407 | 14 | 1673 | 17 |
| Human Fatality | 69510 | 0 | 50250 | 502 | 59760 | 598 |
| Total (Million USD) | 0.278 | 0.483 | 0.2 | 0.386 | 0.368 | 0.449 |

As presented in Table 9, the life-cycle costs show both reductions and increases across different categories after the rehabilitation. Damage-related costs, including structural damage and human impacts (minor and severe injuries and fatalities), show a significant decrease across all three building types. This reflects the improvement in seismic safety achieved by reducing interstory drift, which was one of the primary design targets in the rehabilitation strategy. However, some cost components such as non-structural losses and downtime costs have increased. This is particularly evident in the rehabilitated Kindergarten and Block A, where the non-structural and downtime costs even exceed those of the existing

structures. These increases are attributable to higher floor accelerations resulting from the period shift introduced by the added stiffness during rehabilitation. The shift in dynamic characteristics was not originally a design target, as the rehabilitation primarily focused on drift control in line with existing regulatory and funding priorities in North Cyprus. Consequently, these side effects highlight the need for a more integrated approach to seismic rehabilitation, one that simultaneously considers both structural and non-structural performance criteria.

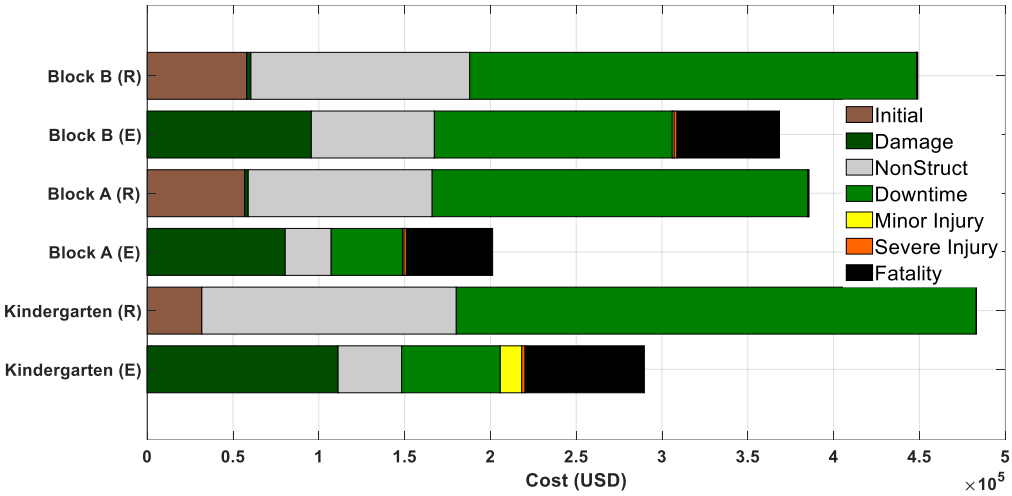


**Figure 20.** Life cycle cost comparison of the buildings for loss scenarios

Although the total cost for rehabilitated buildings is generally higher, this increase is largely driven by non-structural and downtime costs rather than life-threatening consequences. Human-related losses, which are critical from a societal and ethical standpoint, are substantially reduced. For instance, in all three building types, fatality costs drop dramatically—by over 90% in some cases. This suggests that the rehabilitation successfully meets its safety-oriented objectives. Nevertheless, the elevated non-structural losses indicate that if these components were included in the design scope—such as limiting floor accelerations through base isolation or tuned mass dampers—the cost efficiency could have been even more optimized. This raises important considerations for future policy and design frameworks, especially for public buildings such as schools. A visual representation of this cost distribution is provided in Figure 20, where the horizontal stacked bar chart clearly demonstrates the shifting contributions of each cost component between existing and rehabilitated structures.

## 9. CONCLUSION

The seismic rehabilitation of Ataturk Technical High School yielded notable results in improving both safety and cost-effectiveness:

- Seismic Performance Improvement: The retrofitted buildings demonstrated significant reductions in lateral displacements and drift. For example, the kindergarten's roof displacement dropped by 93.5% in the X-direction and 87.7% in the Y-direction. Similar improvements were observed in Blocks A and B, showing reduced displacement and drift ratios, which enhance the building's ability to withstand seismic events.
- Cost-Effectiveness: The rehabilitation costs were substantially lower than building new structures. The cost for retrofitting the kindergarten, Classroom Block A, and Classroom Block B was 5.7%, 14.1%, and 12.1%, respectively, of the cost of constructing new buildings. This makes retrofitting a highly economical option, saving significant amounts of resources while improving safety.
- Reduction in Life-Cycle Costs: The life-cycle cost analysis showed that the rehabilitation significantly reduced structural damage and human-related costs, including fatalities and injuries.

In all three buildings, fatality-related costs decreased by over 90%, indicating a strong improvement in safety and resilience against earthquakes.

- Non-Structural and Downtime Costs: Although some increase in non-structural losses and downtime costs was observed, especially in buildings with higher floor accelerations, these increases were far outweighed by the reductions in structural damage and human harm.
- Holistic Safety Benefits: The retrofitting strategies, which included shear walls and braced frames, not only enhanced structural strength but also improved the overall resilience of the buildings in both primary and secondary seismic events. The rehabilitation ensured that the buildings could meet immediate occupancy requirements even after strong aftershocks.

In summary, the study underscores the effectiveness of seismic retrofitting as a cost-efficient method for improving the safety and resilience of critical infrastructure, especially schools, which play a key role in emergency response and recovery.

**Declaration of Ethical Standards**

The authors declare compliance with all ethical guidelines, including those related to authorship, citation, data reporting, and the publication of original research.

**Credit Authorship Contribution Statement**

The authors contributed to this work as follows: Conceptualization, S.B.; methodology, S.B. and F.K.G.; fieldwork, S.B..; software, S.B.; title, S.B., and F.K.G.; validation, S.B., and F.K.G.; laboratory work, S.B.; formal analysis, S.B. and F.K.G.; research, S.B.; sources, S.B.; data curation, S.B.; manuscript-original draft, S.B.; manuscript-review and editing, S.B. and F.K.G.; visualization, S.B. and F.K.G.; supervision, S.B. and F.K.G.

**Declaration of Competing Interest**

The authors declare that they have no conflict of interest.

**Funding / Acknowledgements**

This research was conducted without any financial support or funding from external sources.

**Data Availability**

The data supporting the findings of this study are available from the corresponding author upon request.

**REFERENCES**

[1] W. Bank, "Global Rapid Post-Disaster Damage Estimation (GRADE) Report- Mw 7.8 Türkiye-Syria Earthquake – Assessment of the Impact on Syria," 2023.

[2] B. Atmaca, M. Emin Arslan, M. Emiroğlu, and A. Can Altunışık, "On the earthquake-related damages of civil engineering structures within the areas impacted by Kahramanmaraş earthquakes," *Journal of Structural Engineering & Applied Mechanics,* vol. 6, 2023, doi: 10.31462/jseam.2023.02098116.

[3] T. P. Doğan, H. Kalkan, Ö. Aldemir, M. Ayhan, M. Böcek, and Ö. Anıl, "Investigation of RC structure damages after February 6, 2023, Kahramanmaraş earthquake in the Hatay region," *Bulletin of Earthquake Engineering,* vol. 22, no. 10, pp. 5201-5229, 2024/08/01 2024, doi: 10.1007/s10518-024-01965-2.

[4] S. Babaei and F. Karimi Ghaleh Jough, "A Comprehensive Evaluation of Tuned Vertical Isolation System for Seismic Risk Mitigation," *Journal of Applied Engineering Sciences,* vol. 14, no. 1, pp. 27-34, 2024, doi: doi:10.2478/jaes-2024-0004.

[5] T. C. C. S. v. B. Başkanlığı, "2023 Kahramanmaraş ve Hatay Depremleri Raporu," T.C. Cumhurbaşkanlığı Strateji ve Bütçe Başkanlığı, Ankara, Turkey2023, Available: https://www.sbb.gov.tr/wp-content/uploads/2023/03/2023-Kahramanmaras-ve-Hatay-Depremleri-Raporu.pdf.

[6] E. Damcı, R. Temür, Z. Kanbir, Ç. Şekerci, and E. Öztorun Köroğlu, "Comprehensive investigation of damage due to 2023 Kahramanmaraş Earthquakes in Türkiye: Causes, consequences, and mitigation," *Journal of Building Engineering,* vol. 99, p. 111420, 2025/04/01/ 2025, doi: https://doi.org/10.1016/j.jobe.2024.111420.

[7] S. Apostolaki, S. Karahan, E. Riga, G. Tsinidis, C. Gokceoglu, and K. Pitilakis, "Seismic performance of tunnels and verification of available seismic risk models for the 2023 Kahramanmaraş earthquakes," *Tunnelling and Underground Space Technology,* vol. 156, p. 106185, 2025/02/01/ 2025, doi: https://doi.org/10.1016/j.tust.2024.106185.

[8] E. Altunsu, O. Güneş, S. Öztürk, S. Sorosh, A. Sarı, and S. T. Beeson, "Investigating the structural damage in Hatay province after Kahramanmaraş-Türkiye earthquake sequences," *Engineering Failure Analysis,* vol. 157, p. 107857, 2024/03/01/ 2024, doi: https://doi.org/10.1016/j.engfailanal.2023.107857.

[9] A. Ihsan Turan, A. Celik, A. Kumbasaroglu, and H. Yalciner, "Assessment of reinforced concrete building damages following the Kahramanmaraş earthquakes in Malatya, Turkey (February 6, 2023)," *Engineering Science and Technology, an International Journal,* vol. 54, p. 101718, 2024/06/01/ 2024, doi: https://doi.org/10.1016/j.jestch.2024.101718.

[10] Y. Yenginar, B. Fidan, and M. Olgun, "A case study: cost-benefit and risk analyses of gabion wall for rockfall protection method in Bozkir, Turkey," (in en), *Konya Journal of Engineering Sciences,* vol. 12, no. 4, pp. 865-885, December 2024, doi: 10.36306/konjes.1510650.

[11] A. E. Sever, P. Usta, E. Şakalak, and C. Ünveren, "Examination of the seismic behavior of the historical Yeşildere bridge," (in en), *Konya Journal of Engineering Sciences,* vol. 12, no. 2, pp. 432-450, June 2024, doi: 10.36306/konjes.1427898.

[12] Ü. İstanbul Teknik, "2023 Şubat 2023 Deprem Son Raporu," İstanbul Teknik Üniversitesi, Istanbul, Turkey2023, Available: https://haberler.itu.edu.tr/docs/default-source/default-document-library/2023_itu_subat_2023_deprem_son_raporu.pdf?sfvrsn=1583fe76_2.

[13] M. Kamanli et al., "February 6 2023 Kahramanmaraş Earthquakes Hatay" Konya Technical University, 2023.

[14] İ. Kazaz, "Evaluation of seismic performance, design and practice of frame-wall buildings in Türkiye after the 6 February 2023 Kahramanmaraş earthquakes," *Journal of Building Engineering,* vol. 99, p. 111557, 2025/04/01/ 2025, doi: https://doi.org/10.1016/j.jobe.2024.111557.

[15] F. Karimi Ghaleh Jough and M. Golhashem, "Assessment of out-of-plane behavior of non-structural masonry walls using FE simulations," *Bulletin of Earthquake Engineering,* vol. 18, no. 14, pp. 6405-6427, 2020/11/01 2020, doi: 10.1007/s10518-020-00932-x.

[16] Z. Qu, F. Wang, X. Chen, X. Wang, and Z. Zhou, "Rapid report of seismic damage to hospitals in the 2023 Turkey earthquake sequences," *Earthquake Research Advances,* vol. 3, no. 4, p. 100234, 2023/10/01/ 2023, doi: https://doi.org/10.1016/j.eqrea.2023.100234.

[17] S. Babaei, A. Habib, M. Hosseini, and U. Yildirim, "Investigating the Inelastic Performance of a Seismic Code-Compliant Reinforced Concrete Hospital Under Long Sequence of Ground Motions Records," in *Sustainable Civil Engineering at the Beginning of Third Millennium*, Singapore, U. Türker, Ö. Eren, and E. Uygar, Eds., 2024// 2024: Springer Nature Singapore, pp. 364-373.

[18] M. Ozturk, M. H. Arslan, G. Dogan, A. S. Ecemis, and H. D. Arslan, "School buildings performance in 7.7 Mw and 7.6 Mw catastrophic earthquakes in southeast of Turkey," *Journal of Building Engineering,* vol. 79, p. 107810, 2023/11/15/ 2023, doi: https://doi.org/10.1016/j.jobe.2023.107810.

[19] T. Y. Altıok, M. Şevik, and A. Demir, "Seismic performance of retrofitted and non-retrofitted RC school buildings after the February 6th, 2023, Kahramanmaraş earthquakes," *Bulletin of Earthquake Engineering*, 2024/08/01 2024, doi: 10.1007/s10518-024-01941-w.

[20] D. De León, L. Esteva, D. Delgado, and J. C. Arteaga, "Optimal reliability to retrofit structures damaged by earthquakes from the perspective of the life-cycle cost," Engineering Structures, vol. 321, p. 118913, 2024/12/15/ 2024.

[21] Y. Kulthanaphanich, R. Permata, and S.-Y. Lin, "Life cycle assessment of integrated energy and seismic retrofits for existing buildings," Journal of Building Engineering, vol. 108, p. 112967, 2025/08/15/ 2025.

[22] X. Yan, N. Rahgozar, and M. S. Alam, "Seismic life-cycle cost evaluation of steel-braced frames: Comparing conventional BRBF with emerging SCVDF and HBF systems," Engineering Structures, vol. 313, p. 118256, 2024/08/15/ 2024.

[23] Y. K. Wen and Y. J. Kang, "Minimum Building Life-Cycle Cost Design Criteria. I: Methodology," *Journal of Structural Engineering*, vol. 127, no. 3, pp. 330-337, 2001/03/01 2001, doi: 10.1061/(ASCE)0733-9445(2001)127:3(330).

[24] C. C. Mitropoulou and N. D. Lagaros, "Life-Cycle Cost Model and Design Optimization of Base-Isolated Building Structures," (in English), *Frontiers in Built Environment*, Original Research vol. 2, 2016-November-07 2016, doi: 10.3389/fbuil.2016.00027.

[25] A. Elenas and K. Meskouris, "Correlation study between seismic acceleration parameters and damage indices of structures," *Engineering Structures*, vol. 23, no. 6, pp. 698-704, 2001/06/01/ 2001, doi: https://doi.org/10.1016/S0141-0296(00)00074-2.

[26] Applied Technology Council. (1985). Earthquake damage evaluation data for California (ATC-13). Applied Technology Council.

[27] Federal Emergency Management Agency. (1992). A benefit-cost model for the seismic rehabilitation of buildings (FEMA 227). Federal Emergency Management Agency.Prota Software. (2018).

[28] OECD (2022), Life-Cycle Costing in Public Procurement in Hungary: Stocktaking of Good Practices, OECD Public Governance Reviews, OECD Publishing, Paris, https://doi.org/10.1787/8d90f627-en.

[29] TBDY 2018. Türkiye Bina Deprem Yönetmeliği. Afet ve Acil Durum Yönetimi Başkanlığı, Ankara

[30] Computers and Structures, Inc. (2023). SAP2000 Integrated Software for Structural Analysis and Design (Version 24). Berkeley, CA: Computers and Structures, Inc. Available at: https://www.csiamerica.com.